

# Characterizing mass, charge, and radius of Lycopodium spores using electrical trapping and optical imaging techniques

Mähring, Marcus<sup>1</sup>

<sup>1</sup>ETH Zürich  
13.11.2021

## Abstract

This article aims to measure the typical mass, charge and radius of charged lycopodium spores by using a Paul trap (quadrupole trap) and elementary experimental techniques such as powder diffraction measurements, high resolution imaging, and terminal velocity measurements in a laminar flow. This was facilitated by laser sampling in an ion trap which was controlled using Raspberry Pi GPIO utilities. The terminal velocity assumption of the particle experiencing laminar flow was also verified, as the Reynolds numbers for the different scenarios all were found to ~~comfortably~~ be  $< 1$ . The experiment found that of a sample size of 15 particles, they have an average mass of  $\bar{m} = (59.5 \pm 4.7)$  ng. The average radius varied, depending on experimental method, between  $(10.51 \pm 0.57)$   $\mu\text{m}$ , and  $(17.8 \pm 1.7)$   $\mu\text{m}$ , from which the typical charge was determined to be about  $249 \pm 49$  thousand unit charges. Finally, the author discusses the underlying distribution of the variables based upon the available data, and finds it requires more thorough investigation and a larger sample size to rectify the assumptions of an underlying normal distribution.

# Contents

<b>1</b>	<b>Introduction</b>	<b>4</b>
1.1	Theory of the trapping configuration . . . . .	4
1.2	The electric field in the center of the trap . . . . .	5
1.2.1	Two parallel plates . . . . .	5
1.2.2	One electrode . . . . .	6
1.2.3	The general case and calculating $q/m$ values . . . . .	7
1.3	Determining radius through diffraction . . . . .	8
1.4	Terminal velocity . . . . .	9
<b>2</b>	<b>Method</b>	<b>10</b>
2.1	Setup, calibration and initial observations . . . . .	10
2.1.1	Setup and calibration . . . . .	10
2.1.2	Loading the trap and initial observations . . . . .	12
2.2	Minimizing micromotion . . . . .	13
2.3	Determination of the average lycopodium spore radius . . . . .	14
2.3.1	Determination through diffraction . . . . .	14
2.3.2	Determination by high-resolution photo . . . . .	14
2.4	Determination of the terminal velocity of lycopodium . . . . .	15
2.4.1	Setup . . . . .	15
2.4.2	Calibration . . . . .	15
2.4.3	Measurements . . . . .	16
<b>3</b>	<b>Results and data analysis</b>	<b>18</b>
3.1	Trap measurements . . . . .	18
3.2	Initial observations . . . . .	18
3.3	Sampling particle at 49, 50, 51 Hz (and continuously) . . . . .	18
3.4	Stability of the trap . . . . .	18
3.5	Minimizing micromotion . . . . .	19
3.6	Measuring radius . . . . .	19
3.6.1	Diffraction . . . . .	19
3.6.2	High resolution image . . . . .	20
3.7	Terminal velocity and the Reynolds number . . . . .	21
3.8	Correction factor and calculating some spore charges . . . . .	22
<b>4</b>	<b>Discussion</b>	<b>24</b>
4.1	Initial observations . . . . .	24
4.2	Sampling particle at 49, 50, 51 Hz (and continuously) . . . . .	25
4.3	Stability of the trap . . . . .	25

4.4	Minimizing micromotion . . . . .	25
4.5	Measuring radius . . . . .	27
4.6	Terminal velocity and the Reynolds number . . . . .	27
4.7	Spore charges . . . . .	28
<b>5</b>	<b>Conclusion</b>	<b>29</b>
<b>A</b>	<b>Safety considerations</b>	<b>30</b>
A.1	Working with electricity . . . . .	30
A.2	Lasers . . . . .	30
<b>B</b>	<b>Code for the Raspberry Pi</b>	<b>31</b>
B.1	Constant beam . . . . .	31
B.2	Software modulation . . . . .	31
B.3	Pulse-width modulation . . . . .	32
<b>C</b>	<b>Data sheet for the laser</b>	<b>33</b>

# 1 Introduction

In this experiment we use a quadrupole trap, a trap made to confine charged particles in space using electric fields. Ion trapping and investigating has been a staple of research in the physical sciences since its introduction and is still facilitating new experimental techniques and studies [10][12]. In this experiment, a Paul trap, laser diffraction and fall in laminar flow are employed to investigate lycopodium spores: namely their average radius, mass, and the charge they carry.

## 1.1 Theory of the trapping configuration

In creating the trapping configuration we must first recall that from Maxwells equations, more specifically due to Gauss' law, the electric fields must be dynamic. I.e. no electrostatic field can satisfy the electric field we require. The solution used is combining an electrostatic field and an oscillating field at a determined frequency  $\Omega$  [10].

In the case where the particle performs a motion which is slow relative to the trapping potential, the average effect of the switching field will be such that it traps the particle at a potential minimum. Thus we can write the total potential as [10]:

$$\Phi(\mathbf{r}, t) = \Phi_{DC}(\mathbf{r}) - \Phi_{AC}(\mathbf{r}) \cos \Omega t$$

with  $\Phi_{DC}$  and  $\Phi_{AC}$  the static and oscillating components of the potential respectively. Now, in a 2D plane we consider the dynamic part and expand it around  $\vec{r} = 0$ , which leads one to a modulated harmonic potential. The movement of the ion in this potential can be separated. For a more thorough derivation, see [10]. This gives the *Mathieu differential equation*:

$$\frac{\partial^2 x}{\partial t^2} = -\frac{q}{m} \frac{\partial \Phi}{\partial x} = \frac{q}{m} (Cx \cos \Omega t)$$

with C a constant determined in the above argumentation. Defining  $\tau = \frac{\Omega t}{2}$  and  $q_x = \frac{2qCx}{m\Omega^2}$  and solving the resulting differential equation in the limit  $q_x \ll 1$ , one gets:

$$x(t) = C_i \cos(\beta\tau) \left[ 1 - \frac{q_x}{2} \cos(2\tau) \right]$$

with  $\beta = |q_x|/\sqrt{2}$ . Noting  $|q_x| \ll 1$  the motion of the particles ~~motion~~ will be dominated by the slower oscillation of  $\omega_s = \beta\Omega/2 \ll \Omega$ , in turn regulated by a smaller oscillation with a higher frequency  $\Omega$ , the oscillation frequency of the AC voltage. The former is the *secular motion* of the particle and the latter the *micromotion* [10].

The secular motion represents the average effect of the fast oscillating electric field. Thus greater displacements around equilibrium due to outside forces lead to greater restoring

forces from the pseudopotential which induces the secular motion.

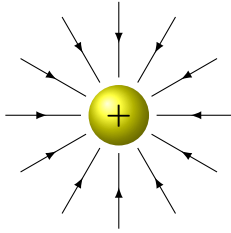


Figure 1: The desired equivalent charge configuration to our trapping setup for a positively charged particle to be trapped in the middle.

## 1.2 The electric field in the center of the trap

In this part a few sample problems are observed to extrapolate some general properties of our trapping configuration. In general we wish to solve the Poisson equation for the electric potential, and then take the negative gradient to find the electric field. For these problems, the Dirichlet boundary conditions (we know the potential on the boundary) will be used to impose uniqueness of the solution [7].

### 1.2.1 Two parallel plates

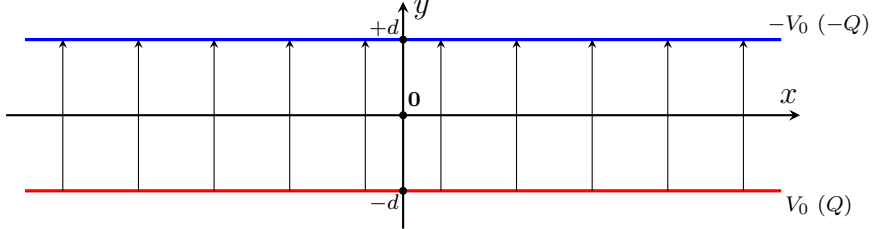


Figure 2: The configuration of two parallel plates with a negative potential on the upper plate and a positive potential of equal magnitude on the lower plate. These plates are assumed to be infinitely long. One should note the symmetry of the configuration: if one should switch the polarity of the two plates, the vector  $\hat{r}$  in equation (1) switches sign.

We have the configuration as follows displayed in figure 2. Here we note that the derivative of our potential is constant, leading us to calculate the derivative of the potential – the magnitude of the electric field – by finding the difference of the potential at the two plates. To find the direction we note that a positive particle in the above configuration will move towards from the upper (negatively charged) plate. In other terms:

$$\vec{E} = \frac{\Delta V}{\Delta r} \hat{r} = \frac{V_0 - (-V_0)}{2d} \hat{r} = \frac{V_0}{d} \hat{r} \quad \hat{r} = \begin{pmatrix} 0 \\ 1 \end{pmatrix} \quad (1)$$

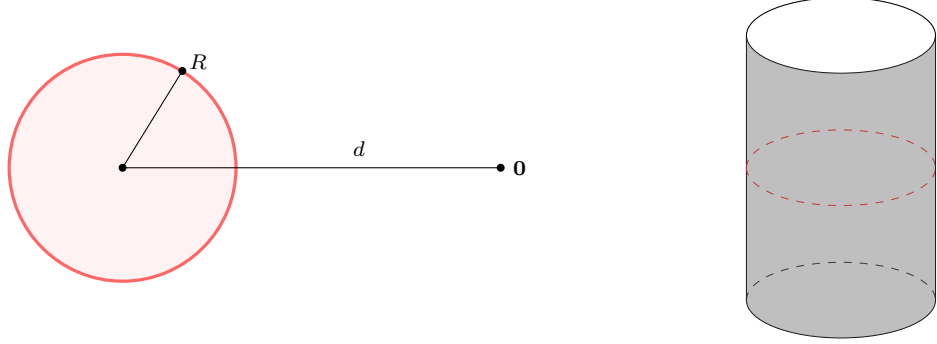


Figure 3: The setup for the one electrode problem. We have a cylindrical symmetry and solve for the potential which this electrode with constant surface potential produces in the plane. Additionally, we impose the potential shall obey  $V(0) = 0$ : it must vanish in the origin.

### 1.2.2 One electrode

Recall the general form of a potential in cylindrical coordinates with cylindrical symmetry (symmetry in the  $z$  coordinate) [7]:

$$V(r, \phi) = a_0 \ln(r) + b_0 + \sum_{m=1}^{\infty} \left[ \left( A_m r^m + \frac{B_m}{r^m} \right) \cdot (C_m \cos(m\phi) + D_m \sin(m\phi)) \right]$$

We now note that at the boundary of our cylinder the solution should match the surface potential, which has no angular part, i.e.  $C_m = D_m = 0 \forall m$ . Thus, at the boundary:

$$V_0 \stackrel{!}{=} a_0 \log(R) + b_0$$

With  $R$  being the radius of the cylinder. Additionally imposing  $V(d) \stackrel{!}{=} 0$  ( $d$  being the distance to the center of the trap) we get the additional equation:

$$0 \stackrel{!}{=} a_0 \log(d) + b_0$$

Thus implying:

$$a_0 = \frac{V_0}{\log(R/d)} \quad b_0 = -\frac{V_0 \cdot \log(d)}{\log(R/d)}$$

Which gives the solution for the potential:

$$V(r, \phi) = \frac{V_0}{\log(R/d)} (\log(r) - \log(d))$$

and the solution for the electric field ( $\vec{E} = -\vec{\nabla}V$ ):

$$\vec{E}(r) = \frac{V_0}{\log(d/R)} \cdot \frac{\hat{r}}{r} \tag{2}$$

### 1.2.3 The general case and calculating q/m values

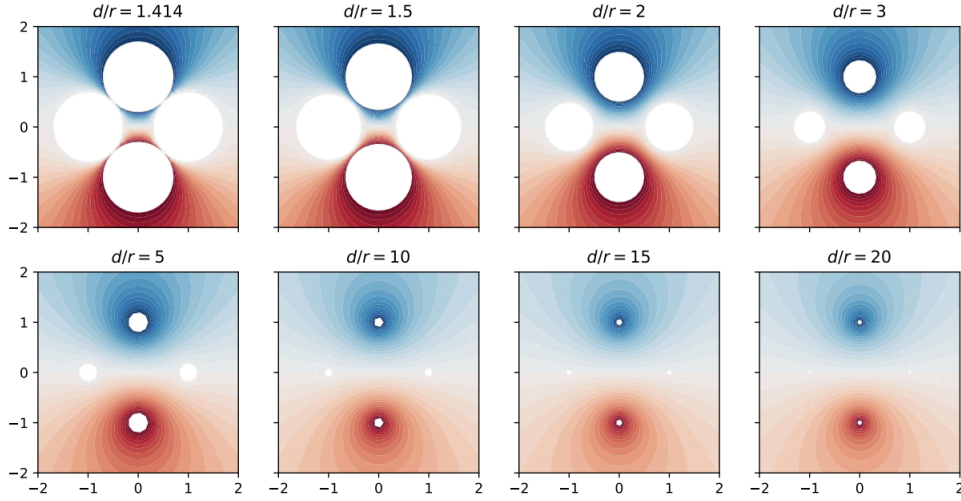


Figure 4: Some simulated electric fields for different trap geometries. [10]

Combining the above considerations, we expect the general E-field in the middle of the trap to be of the form by considering (1) and (2):

$$E_{\text{Mid}} = \alpha \frac{V_0}{d} \quad (3)$$

Where  $\alpha$  is some scaling constant for the trap geometry. However, the trap geometry in the case of four electrodes with constant surface potential is not analytically solvable [7][10]. Thus one must rely on for instance the finite element method (FEM). In figure 4 some sample simulated traps with different distances radii of the electrodes in combination with different distances from the center of an electrode to the center of the trap represented by the  $d/r$  ratio. In section 3 (results) some  $\alpha$  for different  $d/r$  ratios are given together with the first order approximation of the correction factor as in equation (2) (figure 17) [10].

$$mg = qE_c \implies \frac{q}{m} = \frac{g}{E_c} \quad (4)$$

where  $m$  is the mass,  $g$  is the gravitational acceleration,  $q$  being the charge and finally  $E_c$  being the bias electric field in the center of the trap. If we know the bias electric field in the center of the trap, the mass and the distribution of charge per mass coupled with the average mass, we can approximate the charge of the individual (clusters of) particles.

$$q_{\text{Particle}} = \bar{m} \frac{g}{E_c} \quad (5)$$

### 1.3 Determining radius through diffraction

Let  $R$  denote the average radius of the particles we wish to measure,  $R_A$  the radius to the first minimum of the airy disc. For future convenience we also define  $D$  as the distance from the "aperture" / sample to the screen and  $H$  as the hypotenuse in the right hand triangle formed by  $R_A$  and  $D$ .

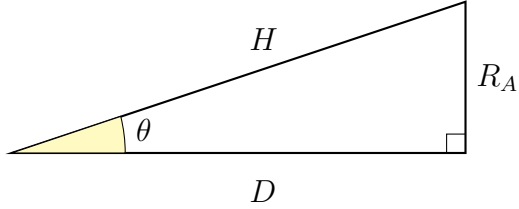


Figure 5: The geometrical setup of the diffraction experiment.

By analyzing the zeros of the first order Bessel function we can find an expression linking the position of the first minimum to the geometry of the setup and the quantities  $\lambda$  and  $R$  [10] [15]:

$$\sin \theta \simeq 1.22 \frac{\lambda}{2R} \quad (6)$$

where 1.22 approximately is the first zero of the first order Bessel function  $J_1(x)$  divided by  $\pi$ . Due to 1.22 being an excellent approximation of this number<sup>1</sup> no distinction shall be made in following.  $R$  is the average radius of the particles in the sample and  $\lambda$  the wavelength of the laser.

To find an expression of the radius of the spores, we employ a common approximation used in conjunction with Fraunhofer diffraction: small angle approximation. Here we assume  $\theta \approx 0$ , which is exactly the case if  $D$  is big in relation to  $R_A$ , defined in figure 5:

$$\sin \theta \approx \tan \theta = \frac{R_A}{D}$$

Thus the equation to solve for  $R$  becomes:

$$R \simeq \frac{1.22\lambda D}{2R_A} \quad (7)$$

---

<sup>1</sup> $||1.22 - x_0/\pi|| \sim 10^{-4}$ , with  $x_0$  the first zero of  $J_1(x)$ .

## 1.4 Terminal velocity

For a particle falling in laminar flow<sup>2</sup> (relatively slowly, keeping the turbulent forces low) the drag of the particle is given by Stokes' law [14]:

$$F_d = -6\pi\mu Rv \stackrel{!}{=} -mg \quad (8)$$

where  $\mu = 1.8 \times 10^{-5} \text{ kg}/(\text{m s})$  is the dynamic viscosity of air,  $R$  is the radius of the falling particle and  $v$  the velocity. When  $v$  is the terminal velocity, the right side of the equation holds [15]. This equivalent to the following relation at terminal velocity  $v_T$  for the mass,  $m$ :

$$\frac{m}{R} = \frac{6\pi\mu}{g} v_T \quad (9)$$

Additionally, the validity of the above result may be investigated if one can certify that the flow around the falling particle is laminar. The quotient of viscous to turbulent forces may be understood by calculating the Reynolds number for the scenario [10]. If  $Re \ll 1$  for the situation the approximation that there is no turbulent flow is valid, and thus we can apply equation (8) [14].

$$Re = \frac{2\rho v_T R}{\mu} \quad (10)$$

Here  $\rho = 1.2 \text{ kg}/\text{m}^3$  is the density of air at atmospheric pressure and  $v_T$  the terminal velocity [10] [14].

The mass and size (radius) of were estimated to be  $m = 2.5 \mu\text{g}$  and  $r = (25 \pm 10) \mu\text{m}$ . If this estimate of the radius is found to be true, and  $v_T$  be of the order  $\sim 300 \text{ mm/s}$ , the Reynolds number should satisfy the condition  $Re \sim 0.1 \ll 1$ , thus implying a laminar flow, in which case Stokes law is valid [14].

---

<sup>2</sup>Note that this only holds for particles with radii  $< 1 \mu\text{m}$ . If the radius is lower, the non-continuum of the gas medium becomes apparent and correction terms are needed [14].

## 2 Method

The experimental method was divided into distinct parts each aiming to determine a certain characteristic of the lycopodium particles to facilitate the ultimate determination of the charge. First, a general outline of the overarching methods describing the general steps which are employed to determine the lycopodium spore charge.

### 2.1 Setup, calibration and initial observations

#### 2.1.1 Setup and calibration

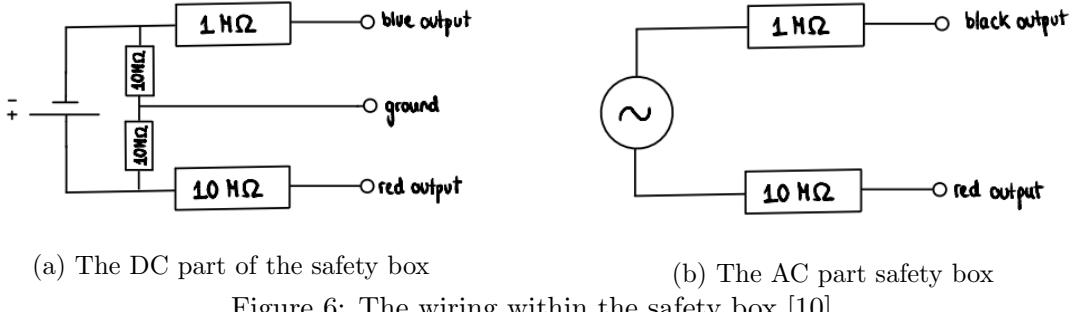


Figure 6: The wiring within the safety box [10]

For the experiment, a variac and a DC power supply were mounted to a safety box. Firstly, the electrodes lying in the horizontal plane of the trap were then both wired to the AC output of the safety box, effectively wiring them to the variac. Secondly, the bias electrodes in the vertical plane were wired to the DC output of the safety box with the upper being connected such as to carry negative current and the lower plates carrying positive current. This allows compensation of gravity later in the experiment by applying a bias electric field in the trap. Finally, the end-caps were all attached to the positive current, enabling the trapping of a positively charged particle.

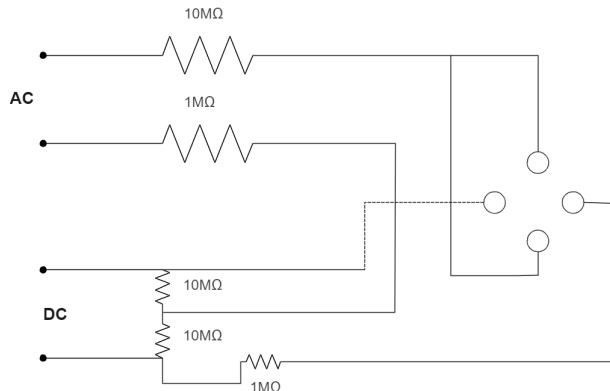


Figure 7: The wiring configuration of the bias section of the rods. Note that the high resistance resistors visible in the schematic belong to the safety box, in effect limiting the maximum current which could flow through an experimenters body. [10]

One should note that this configuration traps a *positively* charged particle, but in the case that one needs to trap a negative particle, the end-caps and the bias' (center segments) voltages signs should be switched. The effect of these modifications is that we create a trapping configuration for the particle in the middle of the trap and again allow compensation for gravity by applying a positive voltage.

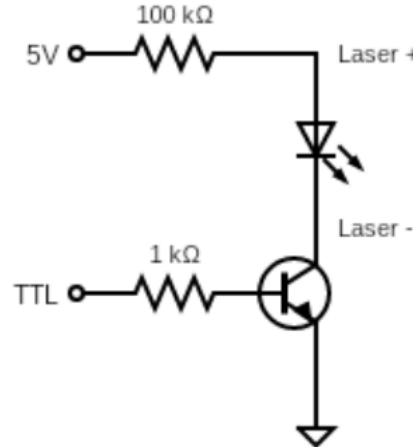


Figure 8: The driver circuit for the laser

Following the setup of the trap, the laser was connected to the driving circuit (see figure 8). The driving circuit consists of a 5 V connection from a Raspberry Pi GPIO header to a resistor of  $100\text{ k}\Omega$  and a transistor. The other end of the transistor was attached to a 3.3 V GPIO output pin (GPIO pin 13) which offers normal digital output as well as pulse-width modulation (PWM), allowing us to trigger the laser via the Raspberry Pi, effectively using the transistor as a switch.

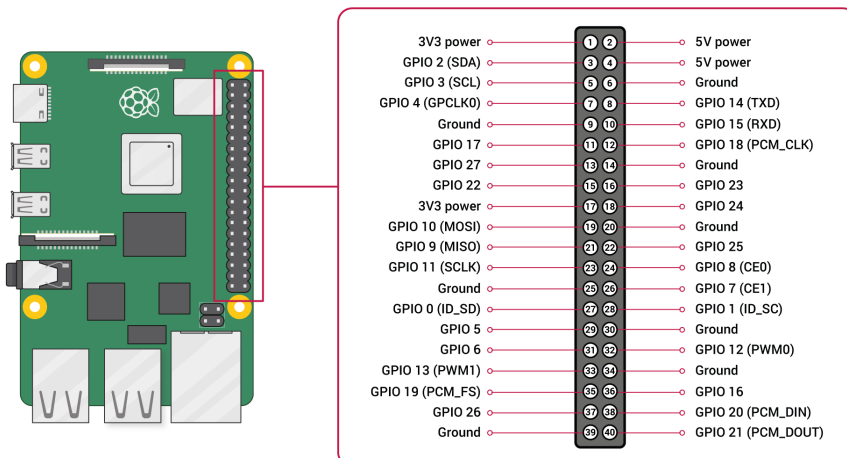


Figure 9: The general layout of the GPIO on the Raspberry Pi model 3b+. Note the pulse-width modulation (PWM) support on GPIO 13. [2]

The additional resistors described above serve the purpose of restricting the effective potential over the laser to allowed levels –  $\leq 3.3$  V – as well as regulating the current to the allowed range of  $\leq 25$  mA (see appendix C for the data sheet of the laser) [10]. One should note that the Raspberry Pi GPIO header provides a maximum of 16 mA per pin, with a total of 50 mA being able to be provided over the entire header at any given moment [2].

After this was done the laser was mounted on the trap and calibrated by adjusting ~~the positioning of the laser~~ to maximize the amount of light let through holes in the trap mount, thus aligning the beam-axis of the laser with the trap center.



Figure 10: The camera mounted to look between the bias electrodes to observe the particles in the middle. The part of the upper electrode where the wire is mounted distinguishes between the bias and endcap parts of the electrode.

Then a see-through plastic wind-shield was set in place over the setup to assure that trapped particles would not be pushed out of the trapping configuration due to external factors such as ventilation or movement in the laboratory. The shield also acts as additional protection for the operator of the setup by covering otherwise exposed wiring and current-carrying electrodes. Finally a Raspberry Pi camera was focused on the trap center where the particles are to be trapped.

### 2.1.2 Loading the trap and initial observations

Before loading the trap the electricity was shut off and the variac was set to 0% of its maximal voltage and then plugged in. To load the trap a few steps were observed. After setting the AC voltage to  $(220 \pm 5)$  V (oscillating at a frequency of 50 Hz) and the DC

voltage to  $(30.0 \pm 0.5)$  V<sup>3</sup>, a small Teflon stick was rubbed against a piece of cloth to induce a surplus charge. This stick was then dipped in a small pooling of lycopodium powder, making the powder (spores) stick to the stick by electrostatic attraction. The stick with the attached lycopodium was then inserted into the trap through an opening in the windshield and was shaken slightly as to get some powder (spores) trapped in the field.

Subsequently two different methods to observe the particles were investigated. Firstly the laser was kept on continuously while observing the particles and afterwards the laser was flashed at a frequency of 49 Hz, 50 Hz and 51 Hz for 1 ms, effectively implemented by using a run-time  $T = 20$  ms at a 5% duty cycle.

## 2.2 Minimizing micromotion

To measure the mass / charge distribution, one can note that as mentioned in section 1 a particle outside of the natural zero of the pseudo-potential will oscillate at a higher rate due to the bigger restoring forces. Thus, by bringing the particle closer to the pseudo-potentials center – effectively compensating for gravity – we can get determine  $q/m$  via equation (4).

The trap stability first tested by observing a singular particle in the trap, while slowly lowering the AC voltage – weakening the trap stability – the DC voltage on the bias plates were then adjusted to minimize the micromotion of the particle. Importantly, the maximum voltage which could be delivered by the DC source was around 32.5 V, imposing a restriction on which particles could be effectively minimized, as some particles may have needed a greater restoring potential. What this means in practice illuminating the particles with a continuous beam and then observing the trace of the particles motion in the field. This trace was observed through the pi camera to obtain a more precise view thereof. The trace was then minimized by adjusting the DC voltages.

The minimization of the micro-motion was done by noting that the sensitivity to the particles position on the z-axis increases when the overall trap stability is lowered: the AC voltage is lowered. The procedure consisted of slowly lowering the AC voltage slightly and when a change in the particles oscillation was detected, the DC voltage was adjusted accordingly to re-minimize this oscillation. This was repeated until the particle escaped the trap due to the weak trapping (AC) voltage. Finally, the last DC value was noted.

---

<sup>3</sup>Note that these estimates are relatively unimportant, as the values of AC 220 and 30 are a starting point, indicating a good range for the trapping configuration.

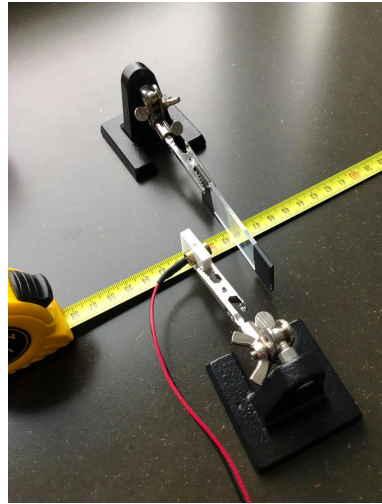


Figure 11: The laser mounted to illuminate the spores with the tape measure indicating the beam axis. Note how the sample and the laser are suspended off the table to project a more complete airy pattern on the screen.

## 2.3 Determination of the average lycopodium spore radius

In this section the determination of the average radius is conducted in two separate attempts: once using diffraction at the scattered lycopodium powder, and once taking a high resolution photograph of the spores and a reference.

### 2.3.1 Determination through diffraction

Lycopodium was sandwiched between two glass plates. This was then suspended in front of the laser held by a small gripping claw aligning the beam axis of the laser parallel to the table to ensure that one could not accidentally look into the laser. The sample was held at a constant distance of  $(50.0 \pm 0.4)$  cm and the wavelength of the laser was read from the data sheet to be  $(655_{-10}^{+5})$  nm (see appendix C for a complete data sheet), but with a typical output of 655 nm. The airy disc pattern was projected on a millimeter marked disc affixed to the wall with some tape. The distance between two minima was then measured, from which the radius could be calculated. From geometrical considerations, we can now determine the average radius of the lycopodium particles.

### 2.3.2 Determination by high-resolution photo

A photo was taken of the sandwiched lycopodium spores suspended on a platform with contrasting background. The sample was then switched out for an iPhone X, of which a photo was taken as well (see figure 12). Knowing the pixels per inch (PPI) value of the phone, 458, a conversion from pixels on the picture taken with the camera was converted to inches, which in turn was converted to centimeters, here as a function of pixels of the



(a) A photo of the phone screen of the iPhone X.



(b) A photo of the spores.

Figure 12: The first set of pictures used to determine the average spore size. If one sufficiently zooms in on the respective pictures one can in 12a determine how many pixels equate to one inch and in 12b find objects which, with the resolution of the camera as the limiting factor, were determined to be (almost) individual particles, enabling one to measure the radii.

~~image with an output in inches:~~

$$L(P, P_r, \text{PPI}) = P \cdot \frac{P_r}{458} \quad (11)$$

with  $P$  the length in pixels of the object (on the picamera photograph),  $P_r$  the length (in picamera image pixels) of one pixel on the iPhone screen, and finally 458 being the PPI value of the iPhone X [5]. The reference length  $P_r$  was measured twice and the mean was taken as to get a more certain estimate, which was then used in converting the pixel radii into centimeters. The above method was completed twice (with the phone).

## 2.4 Determination of the terminal velocity of lycopodium

### 2.4.1 Setup

To determine the terminal velocity of the lycopodium spores ~~a see through tube was mounted on a base plate perpendicular to the plate with a laser mounted in the lower end of the tube~~. The tube was able to be reoriented ~~depending on need~~ thanks to adjustable screws. The positioning of the base place could also be adjusted by tuning the lengths of the screws. A detailed view of the setup is ~~displayed~~ in figure 13.

### 2.4.2 Calibration

The calibration was done in two steps; in the first step the laser was aligned with the tube and in the second the base plate was oriented such that the tube/beam axis was collinear to gravity.

To align the laser with the tube a cap was mounted on the tube with a small hole in it. The laser was then turned on continuously and its orientation in the tube adjusted with

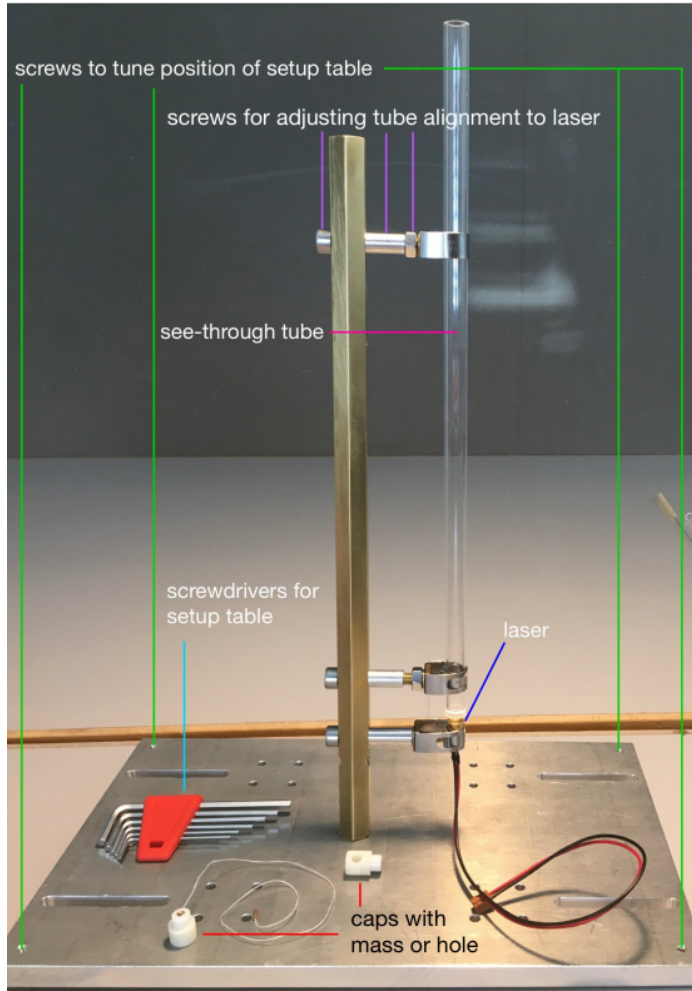


Figure 13: The setup for the terminal velocity experiment. Note how the laser is oriented toward the ceiling, meaning the can drop spores from the upper part of the tube and flash the laser on them to observe their fall. [10]

the screws until a bright red spot was clearly visible on the ceiling, afterwards the laser was turned off for a cap change.

To align the table and the tubing with the direction of gravity, a closed cap with a piece of string attached. The laser was then switched on and the table realigned until the string was continuously illuminated by the beam.

#### 2.4.3 Measurements

To measure the terminal velocity spores were photographed and then the distance traveled in one frame were recorded (pixels), thus allowing the determination of their velocity through  $v = \Delta s / \Delta t$ ; the idea being that if the particles fall for long enough, the terminal velocity will be recorded at the bottom of the tube. For reference to convert this value in [pixels / second] a pendulum of known dimensions was included in the shot, namely the diameter of the weight:  $(2.00 \pm 0.05)$  mm. In figure 14 the final setup is displayed with the camera.

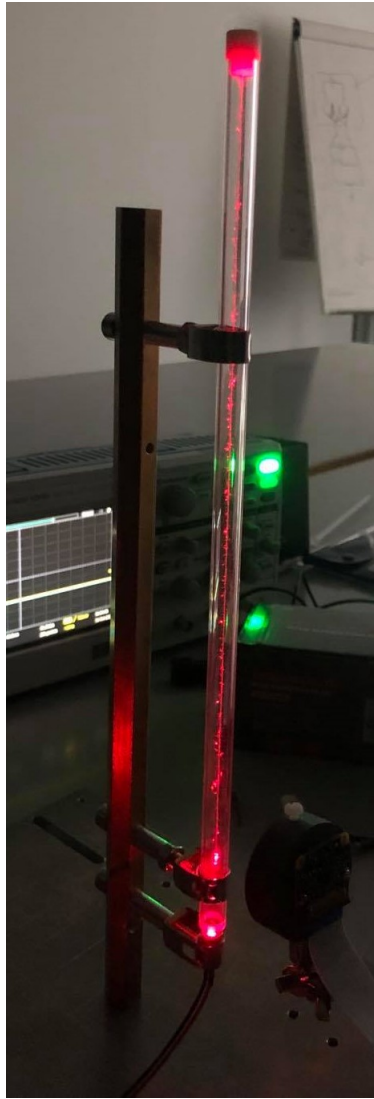


Figure 14: The setup during calibration of the camera with the continuous laser beam.

The particles were then recorded while falling and the laser was pulsed at different frequencies and different duty cycles. Additionally the Pi-cameras ISO values and frame rate were adjusted to better capture the falling spores. The cameras exposure time was set to 500 ms and the framerate was then (depending on measurement series) varied between 10 and 30 FPS.

The first measurement series was done at 10 FPS with a total time-interval of 1 s with a duty cycle of 5% and a pulse frequency of 30 Hz.

The second experiment was done at 20 FPS with 1 s with a duty cycle of 5% and at a frequency of 50 Hz. Some sample code for modulating this signal with PWM and software-driven functionality to output a simple wave [4].

By comparing the pictures taken by these two measurements, conclusions pertaining to the optimal settings for the experiment could be drawn.

## 3 Results and data analysis

### 3.1 Trap measurements

The trap dimensions were measured to be  $r = (3.00 \pm 0.25)$  mm (radius of the electrodes) and  $d = (4.00 \pm 0.25)$  mm ( $d$  being the distance from the center of the trap to the middle of an electrode). This gives the proportion of the trap equal to:  $d/r = 1.33 \pm 0.14$ .

The error propagation can be derived as follows:

$$\sigma_{d/r} = \frac{1}{r} \sqrt{\frac{d^2}{r^2} \Delta r + \Delta d} \quad (12)$$

Here  $\sigma_{...}$  is the standard deviation of the random variable in the subscript and  $\Delta_{...}$  is the variance of the variable ( $\sigma_{...}^2 = \Delta_{...}$ ). This convention will be retained for the rest of the report.

### 3.2 Initial observations

The particle was successfully trapped and one could clearly observe several bright red spots in the middle of the trap illuminated by the laser. Additionally a fast oscillation in the transverse plane with occasional bigger displacement collinear to the beam axis. The particle was observed to be positively charged as it was trapped by the described configuration in section 2.

### 3.3 Sampling particle at 49, 50, 51 Hz (and continuously)

As mentioned, while using a continuous beam traces from the particles were observed. While flashing the laser the particles' individual oscillatory motions were observed, but no discernible difference could be observed between the different frequencies.

### 3.4 Stability of the trap

The stability of the trap for the one particle was recorded for one individual particle to escape the trap at an AC value of 130 V and DC value of 30 V. This was in practice repeated 15 more times in the next part, as the particles escaped the trap every time.

### 3.5 Minimizing micromotion

In table 1 the DC values as well minimizing micro-motion for 15 different particles are given as well as the AC values before the particle leaves the trap.

Measurement:	AC [V]	DC [V]
1	150	14.5
2	80	31.5
3	90	30.5
4	70	27.2
5	120	16.1
6	0	20.3
7	90	25.4
8	85	25.3
9	75	26.8
10	130	29.1
11	125	22.7
12	90	19.9
13	60	29.3
14	105	23.6
15	85	27.5

Table 1: 15 measured values for some distinct separate particles. All DC values are recorded with the same degree of accuracy: about 0.05 V, and analogously the AC values with an accuracy of about 5 V



For the  $q/m$  values the error propagation of equation (4) is:

$$\sigma_{q/m} = \frac{1}{E_c} \sqrt{\frac{g^2}{E_c^2} \Delta E_c + \Delta g} \quad (13)$$

### 3.6 Measuring radius

#### 3.6.1 Diffraction

The distance to the "screen" (measurement area) was as mentioned in section 2 measured to be  $(50.0 \pm 0.4)$  cm and the typical wave-length was about  $(655 \pm 5)$  nm. The distance *between two minima* on the screen were measured to  $D = (3.8 \pm 0.2)$  cm, meaning the radius from the center of the airy disc to the first minima is  $R_A = (1.9 \pm 0.1)$  cm.

The measured value for the radius was calculated to be  $(10.51 \pm 0.57)$   $\mu\text{m}$ .

The error for the distance of the screen was approximated from the fact that we could, in theory, measure to an estimated accuracy of 0.1cm but in practice we could only be precise within a margin of about double that distance. This uncertainty was doubled again as we could not exactly determine the position of the sample on the beam line. On

the millimeter marked screen, the uncertainty was estimated to consist of 0.1cm on each side of the airy pattern. The uncertainty in the wave length was estimated to be about 5nm., thus keeping it in range of the possible wave-lengths on the data sheet about the typical output. The error propagation using small angle approximation is as follows:

$$\sigma_R \simeq \frac{1.22}{2R_A} \sqrt{D^2 \Delta \lambda + \lambda^2 \Delta D + \frac{\lambda^2 D^2}{R_A^2} \Delta R_A} \quad (14)$$

### 3.6.2 High resolution image

The mean radius from the first image was  $(17.8 \pm 1.7) \mu\text{m}$  and for the second image  $(17.6 \pm 3.7) \mu\text{m}$ . The complete data can be seen in table 2.

Particle	Radius (set 1) [ $\mu\text{m}$ ]	Radius (set 2) [ $\mu\text{m}$ ]
1	$24.7 \pm 4.8$	$13.4 \pm 4.0$
2	$24.7 \pm 3.6$	$13.4 \pm 3.0$
3	$21.0 \pm 3.4$	$19.0 \pm 4.8$
4	$16.5 \pm 3.2$	$17.0 \pm 5.6$
5	$21.0 \pm 3.4$	$19.0 \pm 4.8$
6	$16.5 \pm 2.0$	$17.0 \pm 4.5$
7	$13.0 \pm 1.8$	$25.5 \pm 7.8$
8	$10.5 \pm 1.7$	$13.4 \pm 4.0$
9	$13.0 \pm 1.8$	$25.5 \pm 7.8$
10	$16.5 \pm 2.0$	$13.4 \pm 5.2$

Table 2: In this table, ten measured radii from the respective pictures are given in micro meters. The errors were determined individually for each particle, as for some it was more clear than for others where the particle ended propagated together with the uncertainty for the length of one pixel on the iPhone. Here the resolution of the camera was the limiting factor. Note how some nominal values are the same but with different errors. The cause being that some clusters were better resolved than others.

For the error propagation one should note that the uncertainty in PPI is zero (or at least close to zero in relation to the other errors in the experiment), leading to the removal of one term.

$$\sigma_L(P, P_r) = \frac{1}{\text{PPI}} \sqrt{\frac{PP_r}{\text{PPI}^2} \Delta \text{PPI} + P^2 \Delta P_r + P_r^2 \Delta P} \stackrel{\sigma_{\text{PPI}}=0}{=} \frac{1}{\text{PPI}} \sqrt{P^2 \Delta P_r + P_r^2 \Delta P} \quad (15)$$

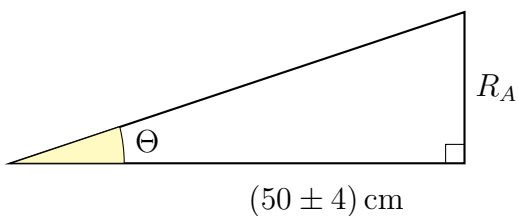


Figure 15: The geometrical setup of the diffraction experiment.

### 3.7 Terminal velocity and the Reynolds number

From observing the taken pictures, one could confirm that the photos taken with a high pulsing frequency respective the frame rate (20 FPS with 1 s, 5% duty cycle and a frequency of 50 Hz) of the camera produced photos where one could observe distinct traces of the particle. Due to the fact that the pulsing frequency was higher than the frame rate, one could also observe several traces after one another. This allowed one to additionally measure the spacing between the end of one trace and the start of another. Using this, one can confirm whether the particle had reached terminal velocity.

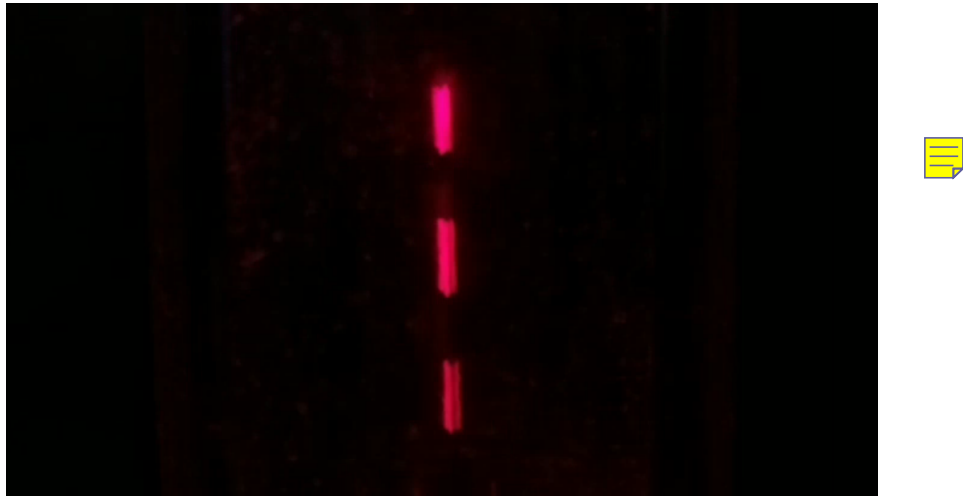


Figure 16: An example of a photo of particles falling in terminal velocity which can be seen by noting the constant distance between the endpoints of one trace to the starting point of the next. We note that this is the same particle which is captured three distinct times. This is logical, as we sample at 50 Hz and capture images at 20 FPS, we expect to find them on average about  $\frac{50}{20} = 2.5$  times.

The terminal velocity was measured for 17 such particles and the mean was determined to be  $(112.40 \pm 40.29)$  mm/s ( $\frac{\delta s}{\delta t}$ ). The error propagation for the terminal velocity follows:

$$\sigma_v = v \sqrt{\frac{1}{\delta s^2} \Delta v + \frac{1}{\delta t^2} \Delta s} \quad (16)$$

The value for the average mass-radius was determined by using the constants given in (8) using an error corresponding to half the last known digit and using the gravitational acceleration  $g = (9.806\,000 \pm 0.000\,005)$  m/s<sup>2</sup>. This was found on the website for the Federal Bureau for Meterology (METAS) [9].

The calculated mass/radius value was then calculated to be  $(38.9 \pm 1.2) \times 10^{-7}$  kg/m using (9). The average mass was then determined by multiplying this quotient with the different measured radii and taking the average of these values. The average mass was thusly determined to be about  $(59.5 \pm 4.7)$  ng. The error propagation for the mass

(see equation (8)) follows:

$$\sigma_m = \frac{6\pi\mu}{g} \sqrt{\frac{R^2 v_T^2}{g^2} \Delta g + v_T^2 \Delta R + R^2 \Delta v_T} \quad (17)$$

Regarding the Reynolds number, as noted in equation (10), it is a function of the radius as well as the velocity. Thus for our different measured radii, we get different Reynolds numbers for the average velocity calculated above. These are displayed in table 3.

	Diffraction	Phone 1	Phone 2
$Re [\cdot 10^{-2}]$	$15.8 \pm 1.2$	$26.6 \pm 2.8$	$26.4 \pm 5.7$
Maximal possible $Re [\cdot 10^{-2}]$	16.9	29.5	32.1

Table 3: Reynolds numbers for the experiment with the diffraction and phone are given in terms of  $10^{-2}$ . Additionally given is the upper bound of the previously mentioned Reynolds numbers, derived from the error of the variables. The values given are rounded to the nearest decimal.

The error propagation for the equation of the Reynolds number is:

$$\sigma_{Re}(v_T, R) = \frac{2\rho}{\mu} \sqrt{R^2 \Delta v_T + v_T^2 \Delta R} \quad (18)$$

### 3.8 Correction factor and calculating some spore charges

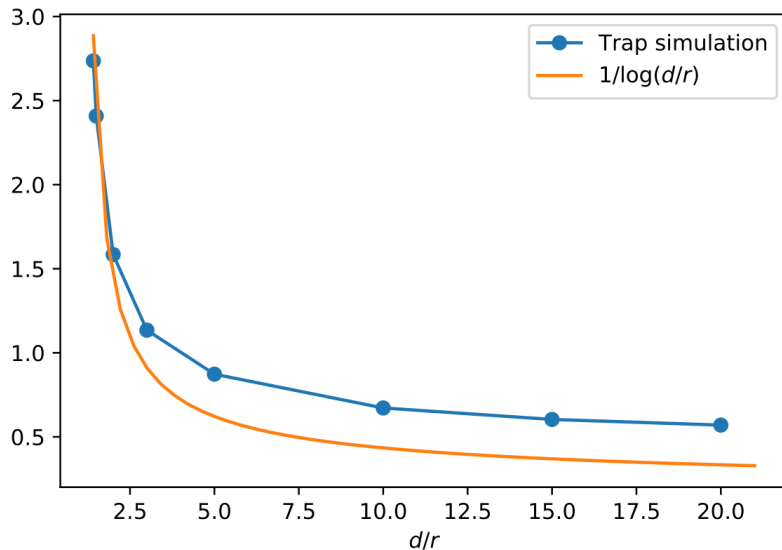


Figure 17: Some simulated  $\alpha$  corrections simulated with the FEM method. Additionally plotted one is the correction factor for one electrode as a function of the  $d/r = d/R$  value [10].

From the calculated  $d/r = 1.33 \pm 0.14$  value one can use the calculate the scaling factor for the geometry by running an FEM simulation on for the given ratio. Alternatively, one can compare with figure 17. To find the  $\alpha$ -value corresponding to the trap geometry from the figure. one simply measures the distance to 2.5 in pixels and the converts  $d/r$  to

a pixel value. One then traces until they hit the blue line which is a linear interpolation from simulated values – at this point we draw a straight line to the y-axis, finding the value of  $\alpha$ . Performing this leads to  $\alpha = 2.50 \pm 0.41$ .

The errors here are calculated by shifting drawn to the blue line with the corresponding errors on the x-axis and finding the  $\alpha$  for these points.

We now calculate some sample charges of particles using equations (3) and (5). These values are given in table 4 with a mean of  $(249 \pm 49)$  ke, with e being the unit charge.

Particle	Charge in Coulomb [fC]	Charge in thousands of unit charges
1	$64.0 \pm 12.0$	$402.0 \pm 77.0$
2	$29.7 \pm 5.7$	$185.0 \pm 36.0$
3	$30.6 \pm 5.9$	$191.0 \pm 37.0$
4	$34.3 \pm 6.6$	$214.0 \pm 41.0$
5	$58.0 \pm 11.0$	$362.0 \pm 70.0$
6	$46.0 \pm 8.8$	$287.0 \pm 55.0$
7	$36.8 \pm 7.1$	$230.0 \pm 44.0$
8	$36.9 \pm 7.1$	$230.0 \pm 44.0$
9	$34.9 \pm 6.7$	$218.0 \pm 42.0$
10	$32.1 \pm 6.2$	$200.0 \pm 38.0$
11	$41.2 \pm 7.9$	$257.0 \pm 49.0$
12	$46.9 \pm 9.0$	$293.0 \pm 56.0$
13	$31.9 \pm 6.1$	$199.0 \pm 38.0$
14	$39.6 \pm 7.6$	$247.0 \pm 47.0$
15	$34.0 \pm 6.5$	$212.0 \pm 41.0$
Mean	$39.8 \pm 7.6$	$249.0 \pm 48.0$

Table 4: Some calculated charges for the observed particles from 1. In the second column the charge in Couloumb is given and in the third the values are given in terms of thousands of unit charges,  $e \approx 1.60218 \times 10^{-19}$  C. All the values have a relative error of 19.21%.

The error propagation for the  $E$ –field is:

$$\sigma_{E_c} = \frac{1}{d} \sqrt{V_0^2 \Delta \alpha + \alpha^2 \Delta V_0 + \frac{\alpha^2 V_0^2}{d^2} \Delta d} \quad (19)$$

and the error propagation for the charge

$$\sigma_q = \frac{1}{E_c} \sqrt{g^2 \Delta \bar{m} + \alpha^2 \Delta V_0 + \bar{m}^2 \Delta g + \frac{\bar{m}^2 g^2}{E_c^2} \Delta E_c} \quad (20)$$

## 4 Discussion

### 4.1 Initial observations

The results found by observing the particles in the trap are as expected from section 1 with the oscillation perpendicular to the beam axis from the displacement out of equilibrium due to gravity. Something unexpected was the bigger non-periodic movements observed along the beam axis. This should not be the case of a singular particle, as the trapping configuration should push the particle back into the middle of the trap by the constant current on the endcaps. A few explanations are possible.

Firstly one reason could be that the airflow in the room and especially that two people were working near the trap. Hypothetically, this should not matter due to the wind-shield, but in practice the wind-shield could not be fit perfectly over the trap due to the wiring. This problem was mitigated by meticulously placing the shield while trying to keep the wiring out of the way. This proved insufficient to completely remove this source of outside influence, as after a short period of time, movement of the wiring and trap from working with it re-displaced the shielding. To solve this in the future one might affix the wiring to the platform on which the trap was mounted and/or add a cable guide to minimize the interaction between the wiring and the shielding.

Secondly it proved impossible to add singular particles with the chosen method of spore charging and trap loading (see section 2). Thus the particles in the trap would experience the electrostatic repulsion from each other. This in combination with that the observed particles did not necessarily carry the same charge as some of them might have gotten more surplus electrons than others. Also, it is unlikely that the observed clusters should consist of singular spores; clusters could therefore in theory carry more charge due to more constituent spores carrying the same charge. Indeed, the latter process could induce a displacement along the beam axis of the manner observed. To counteract this, cluster removal was undertaken: discharging the Teflon stick and using it to catch surplus clusters. This was useful for mitigating the described effect but could not solve it entirely as sometimes when trying to remove the second to last spore, it would be enough to also attract / push the last cluster out of the trapping configuration with either the airflow or direct application of an outside electric field. Also, due to the particles being easily air-borne when applied to the Teflon, it was often the case that particles were stuck around the hole in the shielding and also fell upon the bias electrodes, especially those carrying the AC current. However, these particles cannot affect the trapping of the particles, as they would quickly (within 1/50 of a second) assume the charge of the electrode. Some did in any case wind up getting pushed into the trap by the teflon stick, getting charged and assuming the charge of the instrument, making singular loading more difficult.

This drift, when mitigated, should have no significant effect on the subsequent experiments as they generally do not depend on the particles position in the trap. As long as particles do not get pushed out of the trap at the endcaps due to excessive air flow (movements of the experimenters) or a too significant surplus of charge clusters along the axis. This is important in the case of testing the stability of the trapping, as it may end up pushing the particle out of the trapping configuration prematurely.

## 4.2 Sampling particle at 49, 50, 51 Hz (and continuously)

As mentioned above there was no observable difference between the different sampling rates. This does not correspond to the expected behaviour. The expected behaviour derives from the AC oscillation rate, i.e. the oscillation rate of the particles in the trap of 50 Hz. If we sample the particles oscillation at the same rate as it oscillates, the particle should seem to be standing still and when sampling slightly above/below, one expects to see a slow precession of the particle.

That no difference was observed was primarily theorized to stem from the fact that a software-timed method was used to sample the particles' oscillations. As the time scale at which the sampling was done was of the order  $\sim 1$  ms. The sampling was implemented in Python via the "time" library, more specifically the function "sleep", to wait while the laser was on/off for the duty cycle timing. Python is an interpreted language, and can as such be quite slow, especially function overhead [3] [6] [13]. This means that the de-facto sampling rate / duty cycle was not at the desired 5 ms sampling rate, as the error may have been of the order of the sleep times. For future experiments, a hardware timed solution, such as hardware PWM should be undertaken.

## 4.3 Stability of the trap

The stability of the trap turned out to be better than initially expected, as one could decrease it more than 100 V before the particle started being consequently susceptible smaller perturbations in the trapping. As mentioned, particular care was taken to have as few particles as possible in the trap when this was investigated.

## 4.4 Minimizing micromotion

The minimization of the micromotion was expected to be Gaussian by the author. This assumption was made as the clusters of particles should follow a normal distribution about some mean where the structure is the most stable with deviations depending on the current conditions in the trapping and the particle cluster itself. Assuming a certain amount of charge carried by a particle cluster be proportional to the amount of particles

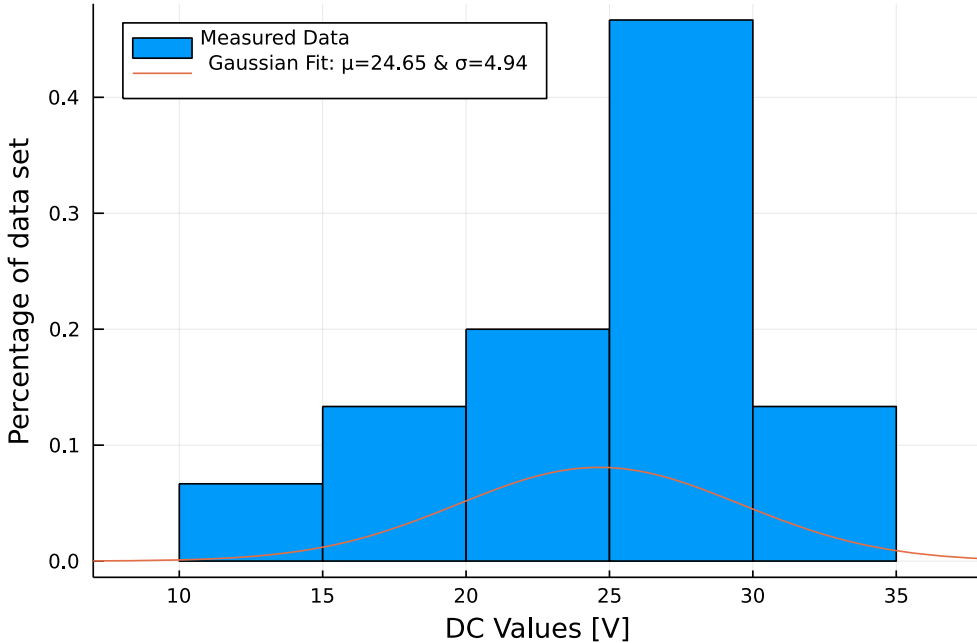


Figure 18: The voltage values from table 4 with a fitted Gaussian. The Gaussian was fitted with the maximum likelihood method, minimizing the maximum likelihood estimator

in the cluster, one may thus infer that the charge/mass configuration (where the mass should also scale extensively with particle number) should be Gaussian. This has additional support from the central limit theorem, saying sequences of random variables from distributions with well-defined primary moments approach a normal curve [8].

In figure 18 a histogram of the measured voltage values from table 4 are given with a normal distribution fitted to the values. The fit was done using the minimization of a maximum likelihood estimator and served the primary purpose of seeing if the histogram generally followed the expected distribution.

Above in section 2 it was mentioned that the maximum value for the DC source was about 32.5 V, which could again contribute to a bias where some values could not be measured. Though, if one fits a normal distribution to the given data and calculates the 95'th percentile, it comes out to slightly over 32.76 V and the CDF for the value 32.5 V is around 94.4%, reducing the greatest possible effect of this equipment restriction to slightly over 6%. In general the histogram suggests a normal distribution but has a significant outlier containing more than 40% of the data ranging between 25 V and 30 V.

One reason which might account for this would be that there might be phenomena related to the formation of the particle clusters which favors configurations which arise at these voltages. However, this is beyond the scope of this study and would have to be done separately.

Another reason could be selection bias. Note how the majority of the data is centered

around the range  $20\text{ V} - 30\text{ V}$ . This might be because as previously mentioned, the charge may scale with the size of the clusters. As particles were partially chosen based how easily they could be distinguished, this could explain the abnormality in the data, as only a subset of the particle would consequently be sampled. Smaller clusters were also often pushed out of the trapping, or otherwise influenced by external parameters, exacerbating the bias.

Finally, considering that the data set has skewness of about  $-0.61$  and a kurtosis of  $-0.62$ , one could also consider that there may be another distribution the particles follow.

## 4.5 Measuring radius

The radius was expected to be around  $(25 \pm 10)\text{ }\mu\text{m}$ , meaning our measurements using the diffraction experiment was about half as big as the expected mean one would expect. The image analysis of the pixels gave a result much closer to this estimated mean. Additionally, in a previous lab, the author measured the radius of lycopodium spores with diffraction and a microscope, which gave radii of  $r_{\text{Diffraction}} = (17.0 \pm 3.5)\text{ }\mu\text{m}$  and  $r_{\text{Microscope}} = (16.0 \pm 2.0)\text{ }\mu\text{m}$  respectively [11], lending further credibility to the measurement using the imaging technique.

The author theorizes that the deviation for the measurement using the laser might have originated from the measurement of distance between the minima on the Airy disc. As mentioned in section 2 this was done with a ruler, which is much too inaccurate to find the minima consistently. Instead a picture should have been taken of the airy pattern, seeing as the screen on which it was projected was already millimeter incremented, a pixel-m conversion could easily have been found. To additionally improve the accuracy of this measurement technique, edge-detection, thresholding, and filtering could have been used to first filter outliers and then find the edges of the airy disc. From this the center of the dark zones (minima) could have been detected more accurately. That the radius from the diffraction experiment lay within none of the expected intervals, could also indicate an underestimate of the errors. The image analysis could also have been improved with the aforementioned tools, but the data matches the expected values quite well.

## 4.6 Terminal velocity and the Reynolds number

The data found for the terminal velocity value seems reasonable at about  $100\text{ mm/s}$ , and mass of  $\sim 60\text{ ng}$  is as such comparable with the estimated mass of  $2.5\text{ }\mu\text{g} = 2500\text{ ng}$ , which again seems reasonable.

The calculated Reynolds numbers for the different determined radii are also well below 1, mostly on the order  $\sim 0.1$  with a mean/standard deviation of  $(22.9 \pm 6.2) \times 10^{-2}$ , in

other words  $< 1$ , making the assumption that the flow is laminar **palatable.**

## 4.7 Spore charges

The average charge was  $(39.8 \pm 7.6) \text{ fC}$ , corresponding to  $(249 \pm 49) \text{ ke}$ , with  $e$  the positive unit charge, which again seems reasonable that on average the equivalent of 250000 additional electrons would be transferred from the Teflon stick to the clusters. That the value in unit charges **is exact** is in a way surprising, as computational errors or other measurement errors would induce computational uncertainty.

The measurements have a relatively high relative error of 19%. To reduce this error, one should according to equation (20) firstly focus on reducing the error in the mass measurement, as the factor  $g^2 \sim 10^2$  dominates the other terms in the error calculation; especially seeing as the error of the voltage is already relatively low.

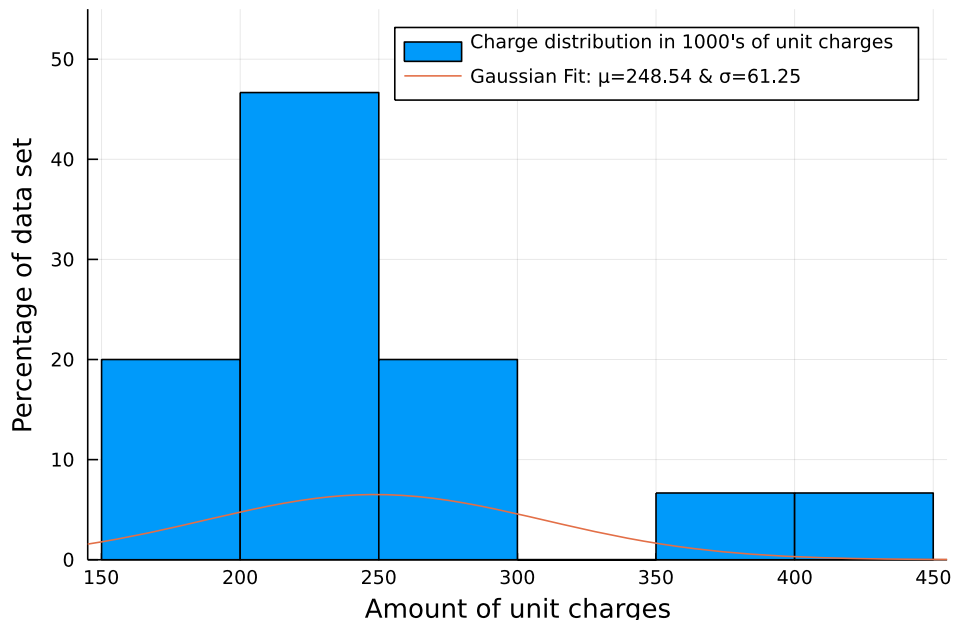


Figure 19: A histogram of the charge data with a fitted normal distribution.

Another important point here is to consider the argumentation pertaining to the normal distribution property of the mass / charge, which should then induce a normal distribution of the charge. As seen in figure 19, this is again not an accurate statement. It is possible, that this would improve with a bigger data set.

This bias may be negated by implementing a way to find the particles, improve the granularity of the DC voltage and take more data. Finally, one should consider if a different distribution may fit better to the charge distribution on the spore clusters.

## 5 Conclusion

In this study, a quadrupole ion trap in combination with elementary experimental techniques were used to determine the average mass, radius and acquired charge of lycopodium spores. For future research these values could be measured more precisely by applying more advanced image processing techniques, improving the range and precision of the DC voltages, and investigating the underlying distribution of the masses and charges.

## A Safety considerations

### A.1 Working with electricity

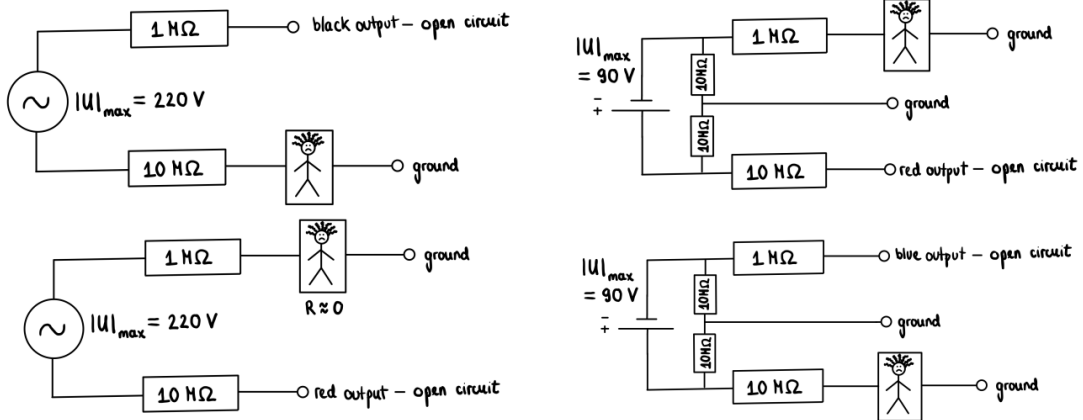


Figure 20: The possible scenarios in which an experimenter could come into contact with live current in this experiment. The scenarios are marked numerically as: 1 (top left), 2 (bottom left), 3 (top right), 4 (bottom right)

Using the situations given in 20 and assuming  $R_{\text{Human}} = 0$ , and that no current flows in the open circuit direction, we can acquire upper bounds for the maximum current which may flow through an experimenters body. In the following equations the I indices refer to figure 20 and the numbering described in the caption.

$$\begin{aligned} I_1 &= \frac{220 \text{ V}}{10 \text{ M}\Omega} = 22 \mu\text{A} & I_3 &= \frac{220 \text{ V}}{1 \text{ M}\Omega} = 0.09 \text{ mA} \\ I_2 &= \frac{90 \text{ V}}{10 \text{ M}\Omega} = 22 \mu\text{A} & I_4 &= \frac{90 \text{ V}}{10 \text{ M}\Omega} = 9 \mu\text{A} \end{aligned}$$

Assuming the safe current is 1 mA, one can clearly see that in all scenarios we are well below the safe current.

When working with electrical equipment, one should also pay special attention to the safe limits for the equipment. This may be mitigated by adding additional resistors, as the operating voltage/current are mostly far below the safe values.

### A.2 Lasers

The laser used in the experiment has enough power to be classed as a class 3 laser though, it is not focused. This means that the effective  $\text{W/m}^2$  is low.

In any case, no jewelry, nor watches should be carried to avoid reflections of the laser light and also avoid looking into the laser.

## B Code for the Raspberry Pi

### B.1 Constant beam

In this listing, a program to continuously deliver a signal to a pin is displayed.

```
import wiringpi

wiringpi.wiringPiSetupGpio() # setup GPIO numbering
wiringpi.pinMode(18, 1)      # declare 18 as an output pin

wiringpi.digitalWrite(18, 1) # write signal "on" to the pin

input("")                      # wait until enter is pressed
wiringpi.digitalWrite(18, 0) # write signal "off" to the pin
```

### B.2 Software modulation

In the following listing, an example of how one can create a software-based solution for flashing the laser at a certain frequency.

```
import wiringpi

T = 1 # total time of one cycle
d = 0.5 # duty cycle: how many % of the time is the laser on?

while True:
    wiringpi.wiringPiSetupGpio()    # setup GPIO
    wiringpi.softToneCreate(17)     # create oscillation on 17

    wiringpi.softToneWrite(17, 50) # start oscillation at 50Hz
    time.sleep(d * T)           # sleep: keep laser on

    wiringpi.digitalWrite(17, 0)  # turn off the laser
    time.sleep((1-d) * T)       # laser off for remainder of cycle
```

For instance if one wants to have the laser on for 5ms, then one should choose  $T = 1$  and  $d = 0.005$  (0.5 %).

### B.3 Pulse-width modulation

```
import RPi.GPIO as Io

Io.setmode(Io.BCM) # we are using BCM ordering
Io.setup(19,Io.OUT) # initialize GPIO19 as an output.

p = Io.PWM(19, 100) # GPIO19 as PWM output, 100Hz frequency
p.start(50)          # create PWM signal with 50% duty cycle
input("")            # wait until enter is pressed
p.ChangeDutyCycle(0) # turn off the modulation
GPIO.cleanup()        # clean up the traces of the program
```

For further documentation, see [1] and [4].

## C Data sheet for the laser

4. High quality lens for copper beam

**PART NO. INDICATIONS**

LC-LMD - 650 - 03 - XX - A

Pin connection:  
 A - Heat sink stand (-)  
 B - Heat sink stand (+)

Output Power: 01 - < 1 mW  
 03 - < 2 ~ 5 mW  
 XX - power set by user

**ABSOLUTE MAXIMUM RATINGS**

Item	Symbol	Rating	Unit
Power supply voltage	$V_{cc}$	3.3	V
Laser Module optical output power	$P_o$	<3 mW	mW
Operation temperature	$T_{opr}$	0 ~ 40	C
Storage temperature	$T_{stg}$	0 ~ 60	C

**ELECTRICAL AND OPTICAL CHARACTERISTICS ( $T_c = 25^\circ C$ )**

Item	Symbol	Min.	Typ.	Max	Unit	Cond
Wavelength	$\lambda$	645	655	660	nm	$P_o <$
Output power	$P_{out}$	01	-	0.6	mW	$V_{cc} =$
		03	2.2	-	mW	$V_{cc} =$
Operation current	$I_{op}$	-	-	15	mA	$P_o =$
Operation voltage	$V_{op}$	-	2.5	-	3.3	Volt
Laser Beam spot size at 10 m				<10 mm		
Divergence angle				1.1 mrad		
Mean time to failure (MTTF) 3 mW 25 C				>10000 hrs		

Page 1

www.laserco.com

Germany and other countries: LASER COMPONENTS GmbH, Phone: +49 8142 2864 0, Fax: +49 8142 2864 11, info@lasercomponents.de  
 USA: LASER COMPONENTS IG, Inc., Phone: +1 603 821 7040, Fax: +1 603 821 7041, info@laser-components.com  
 Great Britain: LASER COMPONENTS (UK) Ltd., Phone: +44 1245 491 499, Fax: +44 1245 491 801, info@lasercomponents.co.uk  
 France: LASER COMPONENTS S.A.S., Phone: +33 1 3959 5225, Fax: +33 1 3959 5350, info@lasercomponents.fr

Figure 21: Data sheet of the laser used for the experiment.

## References

- [1] Ben Croston. Rpi.gpio 0.7.0. Documentation, Independent, 2020.
- [2] Raspberry Pi Foundation. Raspberry pi os. Report, Raspberry Pi, 2021.
- [3] Micha Gorelick and Ian Ozsvárd. *High Performance Python: Practical Performant Programming for Humans*. O'Reilly, Sebastopol, 2020.
- [4] Gordon Henderson. Wiring pi, gpio interface library for the raspberry pi. Documentation, Wiring Pi Project, 2021.
- [5] Apple Inc. iphone x - technical specifications. Report, RAND Corporation, 2021.
- [6] Mohamed Ismail and G. Edward Suh. Quantitative overhead analysis for python. In *2018 IEEE International Symposium on Workload Characterization (IISWC)*, pages 36–47, 2018.
- [7] John D. Jackson. *Classical Electrodynamics*. Wiley, New York, 1998.
- [8] Louis Lyons. *Statistics for nuclear and particle physicists*. Cambridge University Press, The Edinburgh Building, Cambridge, 1986.
- [9] Eidgenössisches Institut für Metrologie METAS. Die gravitationszonen der schweiz. <https://www.metas.ch/metas/de/home/dok/gravitationszonen.html>. Accessed: 07.11.2021.
- [10] D-PHYS: Mordini Carmelo. Quadrupole ion trap. *ETH AP Experiments*, 2021.
- [11] Marcus Mähring and Johannes Eberle. 16, light interference and diffraction effects. From the Praktikum I course, available upon request.
- [12] Wolfgang Paul. Electromagnetic traps for charged and neutral particles. *Rev. Mod. Phys.*, 62:531–540, Jul 1990.
- [13] Guido van Rossum. Google + post. <https://web.archive.org/web/20180919031245/https://plus.google.com/115212051037621986145/posts/HajXHPGN752>. Accessed: 11.11.2021.
- [14] Jing Wang. Lecture script air pollution control ii, environmental engineering. Available upon request.
- [15] Hugh D. Young and Roger A. Freedman. *University Physics with Modern Physics*. Pearson, Essex, 2016.